Gantmakher-Kaner oscillations at 79 GHz in single-crystal copper plates

T. M. Hsu* and G. L. Dunifer
Department of Physics and Astronomy, Wayne State University, Detroit, Michigan 48202
(Received 25 October 1982)

Thin plates of high-purity, single-crystal copper have been investigated with the microwave transmission technique at 79 GHz with the utilization of a magnetic field perpendicular to the sample surfaces and parallel to the ⟨100⟩, ⟨110⟩, and ⟨111⟩ crystal axes. The observed Gantmakher-Kaner oscillations are compared with a theoretical model first proposed by Phillips, Baraff, and Schmidt to explain their data in copper at 35 GHz for a ⟨100⟩ orientation. With the aid of their model we find two classes of signals: (a) those arising from a sharp cutoff of the topological effectiveness, and (b) those due to an extremal helical trajectory. The generally excellent agreement between observation and the predictions of the model for all three crystal orientations confirms the physical significance of the model, although it is lacking a rigorous mathematical derivation.

I. INTRODUCTION

While making a detailed study of the conduction-electron-spin resonance in single-crystal copper at millimeter-wave frequencies,[1] we have had the opportunity of simultaneously monitoring the Gantmakher-Kaner oscillations[2] (GKO) in our samples. These oscillatory signals result from the transmission of microwaves through thin plates of pure metal under the conditions of low temperature and a magnetic field applied normal to the surface of the sample. They are due to the orbital motion of the conduction electrons in the applied field and are observed when the plate thickness is less than or comparable to the electronic mean free path. This paper reports our observations in copper at a frequency of 79 GHz for the magnetic field aligned with the three principal axes: ⟨100⟩, ⟨110⟩, and ⟨111⟩. Earlier reports on copper include the low-frequency ($f \lesssim 30$ MHz) results of Perrin *et al.*[3] and the 35-GHz measurements of Phillips, Baraff, and Schmidt[4] (PBS), the latter being confined to the ⟨100⟩ orientation of the field.

An exact solution for the transmission of the electromagnetic fields through a metal plate under anomalous-skin-effect conditions in the presence of a magnetic field is exceedingly difficult in general. It would have to be a self-consistent calculation that properly accounted for electron spin, the scattering of the electrons at both surfaces of the specimen, and the presence of many-body effects. Rather than attempt such a calculation, we have chosen instead to compare our data with the rather simple model proposed by PBS, which worked surprisingly well in explaining many features of their observations for a ⟨100⟩ orientation. As we shall show the model is helpful in interpreting GKO signals detected for the other two crystalline orientations as well.

II. THEORETICAL MODEL

In the model[4] the plate is divided into two regions—a very thin one at one surface (comparable to the microwave skin depth) where the incident electromagnetic fields drive the conduction electrons and establish a current flow, and a second one (comparable to the electron mean free path and comprising the remainder of the sample) in which the orbiting electrons drift without further interaction with the microwave fields. Under the action of the normal magnetic field H, an electron traces out a helical trajectory across the sample, spiraling at the cyclotron frequency

$$\omega_c = \frac{eH}{m^* c} , \tag{2.1}$$

where m^* is the effective mass of the electron. Those electrons on a thin slice of the Fermi surface, cut normal to the field H, will give rise to a helical distribution of current crossing the sample. For a circularly polarized driving field of frequency ω the helical current distribution has an associated wave vector given by

$$q = \frac{2\pi}{u} = \frac{(\omega \pm \omega_c)}{\bar{v}_H} , \tag{2.2}$$

where u is the pitch of the helix and $\bar{v}_H$ is the average drift velocity of an electron along the field. The $(\pm)$ sign refers to the two possible senses of polarization, with the $(-)$ corresponding to the situation in which the driving field rotates in the same sense that the electrons revolve about the field lines. The

phase of the transmitted microwave field (with respect to the driving field) carried by the electrons across the sample is given by

$$\phi_L = \phi_s + \frac{(\omega \pm \omega_c)_L}{\bar{v}_H} , \tag{2.3}$$

where L is the plate thickness and ϕ_s is an additional phase shift introduced within the skin depths at the two surfaces (where the current is established and where it reradiates power into space at the opposite side).

The total transmitted field is given by summing over all slices making up the Fermi surface whose electrons have sufficient mean free path to reach the second surface. In general, the transmitted fields tend to cancel due to variation of their phases. In certain circumstances, however, the cancellation becomes incomplete giving rise to finite GKO signals which can be detected. By measuring the phase of the transmitted signal as a function of magnetic field, it becomes possible to obtain information about that part of the Fermi surface contributing to the signal.

In order to quantify the ideas in this model, PBS made the following five assumptions.

(i) The transmitted microwave field is proportional to the electrical current flow at the emergent face of the metal plate.

(ii) The current throughout the sample is related to the electric field via a nonlocal magnetoconductivity tensor in the usual way.

(iii) The electric field has appreciable amplitude only within the anomalous skin depth, which can be approximated by a δ function.

(iv) The electrical conductivity tensor can be computed as though the metal plate were infinitely thick, ignoring the scattering of the electrons from its two surfaces.

(v) Any dependence on the frequency or magnetic field of the amplitude and phase of the driving fields within the anomalous skin depth is sufficiently weak that it can be ignored.

Assumptions (iv) and (v) are most open to criticism, although (v) may not be too bad as long as one is not near any resonant conditions for the effective electrons providing the screening within the skin depth. The ability of the theory to match experimental observations will be a direct indication of the overall validity of the assumptions involved.

As a direct consequence of these five assumptions PBS obtain the following expression [Eq. (2.5) in their paper[4]] for the transmitted field:

$$E_\alpha^T = \frac{e^2}{\pi \hbar^3} \sum_{\beta=x,y} \sum_{n=-\infty}^{+\infty} \int_{\bar{v}_H(k_H)>0} dk_H T_{\alpha\beta}(k_H,n) E_\beta e^{iq_n(k_H)L} , \tag{2.4a}$$

where

$$T_{\alpha\beta}(k_H,n) = \hbar m^*(k_H) v_n^\alpha(k_H) v_n^\beta(k_H)^* / \bar{v}_H(k_H) \tag{2.4b}$$

and

$$q_n(k_H) = [\omega + n\omega_c(k_H) + i/\tau]/\bar{v}_H(k_H) . \tag{2.4c}$$

The dc magnetic field $\vec{H}$ is chosen to lie along the z axis, and the polarization α of the transmitted field can be along either the x or y axes. E_β is the amplitude of the driving field at the sample's surface, and k_H is that component of the electron's wave vector along the magnetic field direction. $m^*(k_H)$, $\omega_c(k_H)$, $\bar{v}_H(k_H)$, and $v_n^\alpha(k_H)$, are, respectively, the effective mass, the cyclotron frequency, the average velocity along the magnetic field, and the Fourier coefficients of the transverse velocity components for those electrons whose orbit in $\vec{k}$ space lies in the k_H plane. τ is a phenomenological electron scattering time assumed to be the same for all electrons on the Fermi surface.

Equation (2.4) expresses the transmitted field in much the same form as implied earlier, namely, as a sum over various orbits (each at a fixed k_H) which electrons trace out in $\vec{k}$ space. The field contributed by each orbit has its own spatial helix characterized by the q value given in Eq. (2.4c). The quantity $T_{\alpha\beta}$ is a measure of how effectively the electrons at slice k_H on the Fermi surface extract energy from the driving fields and deliver it to the opposite side of the sample. PBS have labeled this parameter the "topological effectiveness," since it depends crucially on the topology of the Fermi surface and the detailed nature of the electron orbits for a given applied field $\vec{H}$. A new feature which appears in Eq. (2.4) is the sum over n which allows electrons on a given k_H slice to set up q values associated with higher harmonics of the cyclotron frequency. This results from the possibility of having noncircular orbits in momentum space. For a general Fermi surface, as the electron traces out its orbit within a given plane perpendicular to the applied field, its motion can be represented as a Fourier series consisting of the superposition of a number of circular orbits of various sizes occurring at the fundamental cyclotron frequency and integer multiples thereof. It is these higher-frequency circular components

that are able to set up their own spatial helices of current distribution, which are responsible for the $n>1$ possibilities in Eq. (2.4c). The required values of n needed to represent a given orbit depend upon the rotational symmetry of that orbit. In general for m-fold rotational symmetry, the selection rule[3,4] is

$$n=m\alpha\pm 1 , \tag{2.5}$$

where α is any integer or zero and the $+$ or $-$ sign is taken according to the sense of circular polarization that is present in the driving fields.

Equation (2.4) predicts three conditions under which GKO signals can arise due to incomplete cancellation of fields from the various helices. The first condition is the GKO arising from electrons at a *limiting point* on the Fermi surface. This produces a weak GKO which has not been seen in copper, but which is routinely seen[5] in the alkali metals with their spherical Fermi surfaces.

A second possibility arises from a class of orbitals having an *extremal helical trajectory* (EHT). This occurs if, as k_H is swept through its allowed range in Eq. (2.4a), the phases of the various helices pass through an extremum. In the neighborhood of such a k_H (which we shall call k_n) many helices will all contribute together in phase producing a nonzero transmitted field. The condition for this to occur is

$$\frac{d}{dk_H}\mathrm{Re}[q_n(k_H)L]=\frac{d}{dk_H}\left[\frac{\omega+n\omega_c(k_H)}{\bar{v}_H(k_H)}\right]=0 . \tag{2.6}$$

With the use of the relationship[6] that

$$2\pi m^*(k_H)\bar{v}_H(k_H)=\hbar\left[\frac{\partial A}{\partial k_H}\right]_E , \tag{2.7}$$

where $A(k_H)$ is the cross-sectional area of the Fermi surface slice at k_H, Eq. (2.6) can be written as

$$\frac{d}{dk_H}\left[\frac{\partial A}{\partial k_H}\right]_E=\frac{2\pi\omega\bar{v}_H}{\hbar(\omega+n\omega_c)}\frac{dm^*}{dk_H} . \tag{2.8}$$

This is a complicated equation, depending on both the geometry of the Fermi surface and the magnetic field strength, from which it is difficult in general to find k_n. On the other hand, if the effective mass is reasonably constant in this vicinity of k_H (as occurs in the analysis of some of our data), then the preceding equation simplifies to

$$\frac{d}{dk_H}\left[\frac{\partial A}{\partial k_H}\right]_E=0 . \tag{2.9}$$

This relationship depends only on the geometry of the Fermi surface and says that the rate of change of the Fermi-surface cross-sectional area with k_H is extremal at k_n. This is the same condition obtained at low frequencies[2,3] when $\omega\ll\omega_c$. Expanding $q_n(k_H)$ about k_n we have

$$q_n(k_H)=q_n(k_n)+\tfrac{1}{2}q''(k_n)(k_H-k_n)^2 . \tag{2.10}$$

Substituting this into Eq. (2.4) one obtains

$$E_\alpha^T\approx\sum_{\beta,n}\frac{1}{[q''(k_n)L]^{1/2}}T_{\alpha\beta}(k_n,n)E_\beta e^{iq_n(k_n)L} . \tag{2.11}$$

Equation (2.11) shows that the periodicity of the EHT type of GKO signal is due to that particular orbit having the extremal helical trajectory.

As first pointed out by PBS, a third condition which can produce a GKO signal is the sharp *cutoff of the topological effectiveness* (CTE), i.e., a rapid k_H dependence of the quantity $T_{\alpha\beta}(k_H,n)$. Under these conditions a GKO arises whose wave vector is due to that slice of the Fermi surface occurring just prior to the cutoff of $T_{\alpha\beta}$. Figure 1 illustrates straight-line approximations for two types of topological effectivenesses encountered for copper. In Fig. 1(a) $T_{\alpha\beta}$ experiences a sharp cutoff between a and b; while in Fig. 1(b) sharp cutoffs occur between

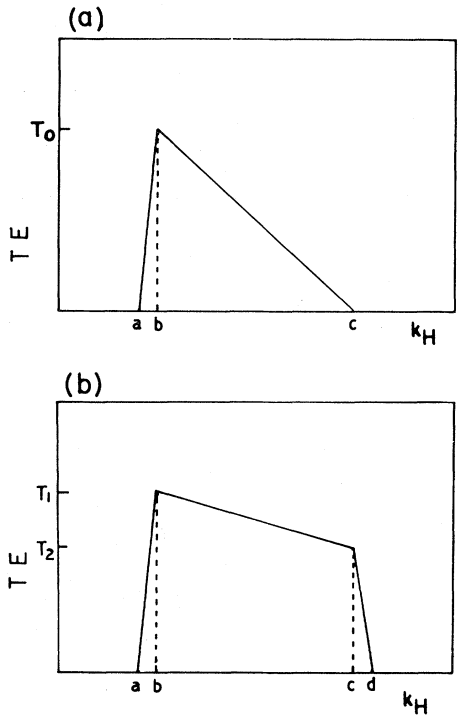

FIG. 1. Straight-line approximations of the topological effectiveness to the types found in copper: (a) that appropriate for the ⟨100⟩ and ⟨111⟩ orientations, and (b) that appropriate for the ⟨110⟩ orientation.

a and b and again between c and d. For the first type of topological effectiveness, one can expand $q_n(k_H)$ to first order about $k_H = b$:

$$q_n(k_H) = q_n(b) + (k_H - b)q'(b) \ . \tag{2.12}$$

Substituting this into Eq. (2.4) one obtains

$$E^T \approx T_0 e^{iq_n(b)L}/q'(b)L \ . \tag{2.13}$$

This type of GKO is thus characterized by the topological effectiveness and phase of those electrons located at the slice of maximum effectiveness. In the same manner, one can show that for the second type of topological effectiveness, Eq. (2.4) becomes

$$E^T \approx \frac{T_1 e^{iq_n(b)L}}{q'(b)L} + \frac{T_2 e^{iq_n(c)L}}{q'(c)L} \ . \tag{2.14}$$

In this situation one expects a superposition of two oscillatory signals with different periods and amplitudes.

For each of the three types of GKO mentioned, an interesting phenomenon is predicted by Eq. (2.4) under the circumstance that the effective mass is reasonably constant,

$$dm^*(k_H)/dk_H \approx 0 \ ,$$

in the vicinity of the orbit responsible for the GKO signal. For this situation, the quantities q' and q'' appearing in the denominators of Eqs. (2.11), (2.13), or (2.14) can have the term

$$\omega + n\omega_c(k_H) + i/\tau$$

factored out in front of the derivative. This leads to a resonant increase in the amplitude of the transmission signal whenever

$$\omega_c(k_H) = -\omega/n \ . \tag{2.15}$$

PBS have called this *cyclotron phase resonance* (CPR) as it is due to a large group of electrons having a range of $\bar{v}_H$ all arriving at the emergent face of the sample in phase with each other when the pitches of their helical current distributions tend to infinity. The observation of CPR immediately allows the determination of the effective mass of those electrons responsible for the GKO signal. In general only those values of n determined by the rotational symmetry of the electrons' orbits [Eq. (2.5)] give rise to resonances in Eq. (2.15). CPR in the limiting-point GKO of sodium and potassium metal has been studied extensively,[5,7] and gives rise to effective masses in close agreement with those measured by Azbel-Kaner cyclotron resonance[8] and the de Haas–van Alphen effect.[9,10] Because of the spherical Fermi surfaces of these two metals, only the $n = 1$ CPR has been reported.

All the GKO signals discussed so far are of the form

$$E^T \approx C(k_n, H)e^{iq(k_n,H)L} \ , \tag{2.16a}$$

where

$$q(k_n, H)L = \frac{\omega + n\omega_c(k_n, H)}{\bar{v}_H(k_n)} L \ . \tag{2.16b}$$

If the orbit contributing to this signal (defined by k_n) is constant, then the phase in Eq. (2.16) will be a linear function of the magnetic field. This produces a sinusoidally varying signal as the magnetic field is swept, with the spacing between oscillations [given by Eq. (2.16b)] being

$$\Delta H = \frac{2\pi c}{neL} m^* \bar{v}_H \tag{2.17a}$$

or

$$\Delta H = \frac{c\hbar}{neL} \left[\frac{\partial A}{\partial k_H} \right]_E \tag{2.17b}$$

making use of Eq. (2.7). ΔH is constant as long as k_n is fixed. This will always be true for the CTE-type GKO but only true for the EHT type when $dm^*/dk_H \approx 0$ in the vicinity of k_n.

III. EXPERIMENTAL TECHNIQUE

The samples consisted of thin plates of high-purity (99.9999%), single-crystal copper oriented with the principle axes ⟨100⟩, ⟨110⟩, and ⟨111⟩ perpendicular to the sample plane. The samples were oriented to within 0.5° of the desired orientation using Laue back-reflection techniques. Most of the specimens were cut from single-crystal rods grown in the laboratory of S. Schultz, although a few were obtained from material purchased from Atomergic Chemical Co. Resistivity ratios ($R_{290\,K}/R_{4.2\,K}$) of the bulk starting material were typically 5000 to 8000. Slices one millimeter in thickness were first cut from the ingots using either a spark cutter or low-speed diamond saw, and the damaged layers at both surfaces were removed by chemical polishing to a final thickness of 0.002 to 0.040 cm. To maximize the resistivity ratio of the samples, they were oxygen annealed[11] for 2—10 h at 900 °C in air at a pressure of 2×10^{-4} Torr.

The GKO were observed using the microwave transmission technique, in which the copper sample makes up a common wall between two microwave cavities tuned to the same resonant frequency. Incident microwaves (up to 100 mW in power) are directed into one cavity where the rf electric fields couple to the conduction electrons of the sample. The other cavity on the opposite side of the sample

acts as a receiving antenna collecting any microwave power radiated from the emergent face of the sample. The transmission spectrometer, which is described in more detail elsewhere,[12,13] operates at 79 GHz and incorporates a liquid-helium-cooled hot-electron InSb bolometer operating in a mixing mode as its microwave detector, giving an overall sensitivity of 10^{-21} W in a one-hertz bandwidth. In order to avoid accidental leakage between the two cavities, indium gaskets were used to seal the sample to the cavities. A dc magnetic field (0—60 kG) is generated by a superconducting solenoid and applied normal to the surface of the sample. Although the temperature of the sample can be varied between 1.3 and 50 K, the results reported here were all taken at 4.2 K, below which the electrical conductivity of copper does not increase significantly.

Both rectangular cavities have identical dimensions and are resonant in the TE_{101} mode. Consequently, the GKO signals are driven by *linearly polarized* electric fields at the incident surface of the sample and are detected at the emergent face by a receiving cavity responding only to a linear polarization (same as that of the transmitting cavity). Furthermore, because the microwave detector is acting as a mixer, using a large reference signal derived from the same source as the driving fields, the final signal is only that component of the transmitted field which is in phase with the reference. Equation (2.16) thus leads to a signal of the form

$$S \approx \sum_{n=-\infty}^{+\infty} C_n \cos[(\omega + n\omega_c)/\bar{v}_H + \phi_n + \phi_0] , \tag{3.1}$$

where ϕ_n is a magnetic-field-independent phase shift introduced at the two surfaces of the sample and ϕ_0 is the phase difference between the driving fields and the microwave reference (adjustable by means of a variable phase shifter in the reference arm of the spectrometer). ω_c and $\bar{v}_H$ are those appropriate for the dominating slice of the Fermi surface.

For the fundamental GKO only $n = \pm 1$ terms are present. For linearly polarized transmission the $n = +1$ and -1 components must be present with equal amplitudes giving

$$S_{\text{lin}} \approx C_1 \cos\left[\frac{\omega L}{\bar{v}_H} + \frac{(\phi_1 + \phi_{-1})}{2} + \phi_0\right] \cos\left[\frac{\omega_c L}{\bar{v}_H}\right] . \tag{3.2}$$

As the magnetic field is swept, this GKO signal is characterized by having an amplitude which is an oscillatory function of ϕ_0, but whose phase is independent of ϕ_0. As first reported by PBS for a ⟨100⟩ orientation, this type of signal is only seen at low fields, and for higher fields becomes that appropriate for circularly polarized transmission. We observe the same effect not only for the ⟨100⟩ orientation but for the ⟨110⟩ and ⟨111⟩ orientations as well. For circularly polarized transmission Eq. (3.1) becomes

$$S_{\text{circ}} \approx C_{-1} \cos\left[\frac{(\omega - \omega_c)L}{\bar{v}_H} + \phi_{-1} + \phi_0\right] . \tag{3.3}$$

This is the polarization which produces CPR and the one we observe experimentally. As the magnetic field is swept, this GKO signal is characterized by a phase which depends linearly on ϕ_0, but whose amplitude is independent of ϕ_0. The appearance of circularly polarized GKO at higher magnetic fields is not predicted by the model of PBS, and its origin is not known. It may not depend entirely on the anisotropy of the Fermi surface since similar behavior occurs to a certain extent in the GKO signals of sodium and potassium at 79 GHz.[14]

IV. RESULTS

For each crystal orientation we will give first the theoretical predictions of the model and then follow with the experimental data. In some cases the data are quite complicated, often displaying more than one type of oscillation at the same time. In general we have only considered those GKO signals in which the periodicity is well defined and constant over a number of cycles (extending at least 5—10 kG in the magnetic field).

A. ⟨100⟩ orientation

For this orientation the ⟨100⟩ crystal axis is normal to the plane of the specimen and parallel to the applied field $\vec{H}$. The necks on the Fermi surface extending along the ⟨111⟩ directions give rise to electron orbits for this geometry which have fourfold rotational symmetry.

1. Theoretical predictions

Figure 2 presents a graph of the orbital parameters needed for the interpretation of the experimental data. Plotted are $m^*(k_H)$, $\bar{v}_H(k_H)$, and $T_{\alpha\beta}(k_H)$ vs k_H/k_{FE}, where k_{FE} is the free-electron wave vector calculated from the density of the conduction electrons. These graphs are produced using the same methods as PBS (Ref. 4) and utilizing Halse's model of the Fermi surface of copper[15] to obtain Fermi wave vectors and velocities. m^* and v_H are obtained by integrating the equations of motion around an orbit. $(\partial A/\partial k_H)_E$ is obtained both directly from the Fermi-surface data and also from

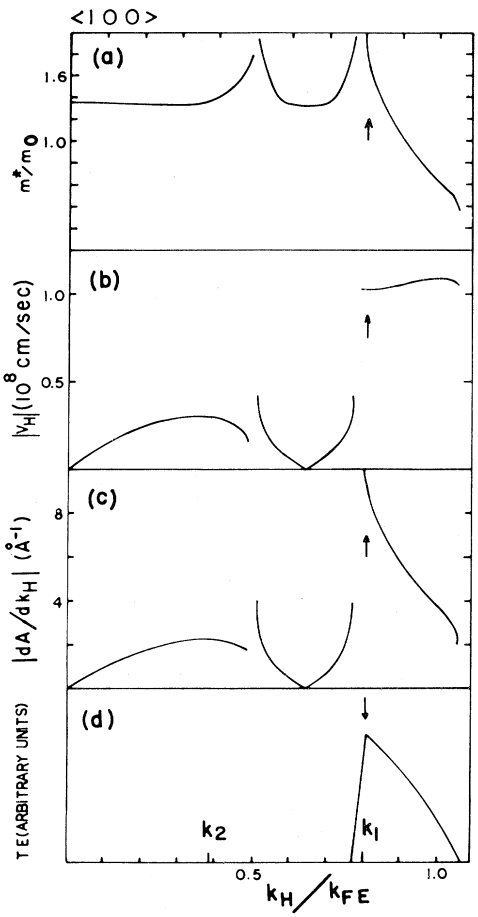

FIG. 2. Fermi-surface parameters for the ⟨100⟩ orientation of copper: (a) the effective mass, (b) the average velocity along the field, (c) the parameter $|dA/dk_H|_E$, and (d) the topological effectiveness (shown for polar electrons only). Arrows at k_1 indicate an orbit leading to a CTE oscillation.

the graphs for m^* and $\bar{v}_H$ making use of Eq. (2.7). This allows a partial check of the computer calculations. Plotted in Fig. 2(d) is

$$T^1_{xx}+iT^1_{xy}\equiv T_1 \tag{4.1}$$

which is the appropriate topological effectiveness for circularly polarized transmission. Orbits which lie in the range

$$0.5\lesssim k_H/k_{\rm FE}\lesssim 0.8$$

encounter the necks and are continuous only in the extended zone scheme. Orbits with $k_H/k_{\rm FE}\gtrsim 0.8$ will be referred to as polar orbits, and those with $k_H/k_{\rm FE}\lesssim 0.5$ will be referred to as belly orbits.

From the figure it is clear that electrons on polar orbits have the longest mean free paths directed across the specimen, and, therefore, are most likely to contribute to any GKO signals observed in thick samples. The topological effectiveness for these electrons reaches a peak at $k_1=0.80k_{\rm FE}$ and shows a sharp cutoff below this value. Consequently, one would predict a CTE-type GKO due to this orbit, with oscillations having a period related to $(\partial A/\partial k_H)_E$ given by Eq. (2.17b). $(\partial A/\partial k_H)_E$ is equal to 8.6 Å^{-1} at k_1 (see arrow in figure). Because $m^*(k_H)$ is varying quite rapidly in this region, a CPR for this particular signal is not predicted. According to Eq. (2.13) the amplitude of the oscillations is proportional to $T_0/q'L$. Making use of the fact that $\bar{v}_H$ is approximately constant in the vicinity of k_1, the predicted amplitude becomes

$$T_0/q'L\approx\frac{m^*(k_1)\bar{v}_H(k_1)T_0}{\omega_c(k_1)L}\left[\frac{dm^*}{dk_H}\right]^{-1}, \tag{4.2}$$

which is inversely proportional to the magnetic field and provides an identifying feature for this type of GKO. Because $(\partial A/\partial k_H)_E$ has no extremum for the polar electrons, it is unlikely that they will produce an EHT variety of GKO.

On the other hand, $(\partial A/\partial k_H)_E$ does pass through an extremum for the belly orbits at $k_2=0.39k_{\rm FE}$. Furthermore, because $m^*(k_H)$ is nearly constant in this region, we expect an EHT-type GKO due to the extremal orbit at k_2 [Eq. (2.9)] and an associated CPR for

$$n=1,3,5,7,\ldots$$

[as predicted from Eq. (2.5) and the fourfold rotational symmetry of the orbits]. The period of this oscillation is again determined by $(\partial A/\partial k_H)_E$, which from Fig. 2 is 2.2 Å^{-1} at k_2. This second class of GKO should appear in thinner samples for which electrons on the belly orbits can traverse the specimen prior to scattering. From Eq. (2.11) the amplitude of the expected signal is proportional to $(q''L)^{-1/2}$. Assuming the effective mass to be constant at k_2, we also have $d\bar{v}_H/dk_H=0$ at this point giving

$$(q''L)^{-1/2}=\bar{v}_H(k_2)\left[[\omega+n\omega_c(k_2)+i/\tau]L\times\left|\frac{d^2\bar{v}_H}{dk_H^2}\right|\right]^{-1/2}. \tag{4.3}$$

The real part of Eq. (4.3) gives rise to a series of symmetric peaks occurring at $\omega_c=-\omega/n$, which are the CPR signals predicted.

2. *Experimental observations*

Figure 3 shows the transmission signal for a specimen 9.5×10^{-3} cm in thickness and having the rather low resistance ratio of 1200. The spectrum is

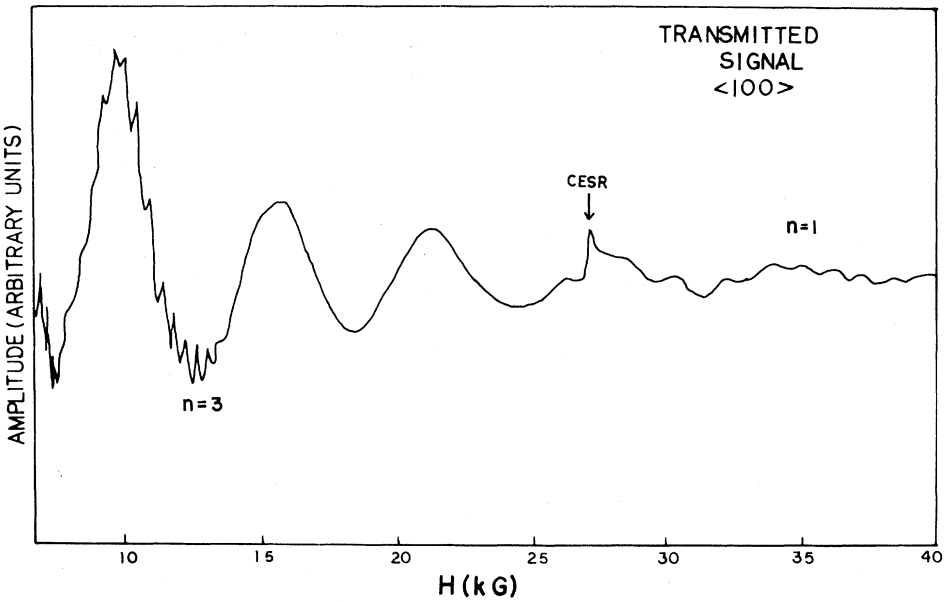

FIG. 3. Transmitted signal as a function of the dc magnetic field for a ⟨100⟩ sample. Sample thickness is 0.0095 cm, and the resistance ratio is 1200.

dominated by an oscillatory signal having a constant period of about 6 kG which decreases in amplitude with increasing magnetic field. "Fine-structure" oscillations occur at magnetic fields near 12 and 35 kG. The conduction-electron-spin resonance (CESR) signal is seen in the vicinity of 27.5 kG. The dominant oscillation is identified as the CTE-type GKO due to the orbit at k_1 in Fig. 2. Putting the measured spacing between oscillations in Eq. (2.17b), one calculates $(\partial A/\partial k_H)_E = 8.76$ Å^{-1} at k_1 in close agreement with the prediction of the model. Figure 4 shows that the amplitude of the oscillation is nearly inversely proportional to the magnetic field strength as predicted by Eq. (4.2). The "fine-structure" oscillations are identified as CPR ($n=1$ and 3) of the EHT-type GKO due to the orbit at k_2 in Fig. 2. They are sufficiently weak that no attempt was made to do a precise analysis on them for this sample.

Figure 5 shows the transmission signal for a thinner sample,

3.8×10^{-3} cm ,

with approximately the same resistance ratio. CPR signals now dominate the spectrum with the CTE oscillations providing a weaker and more slowly varying background. This is as expected. Once the belly electrons are able to traverse the sample without scattering, their stronger coupling to the driving fields (greater topological effectiveness) combined with the CPR enhancement causes them to dominate the GKO spectrum. CPR signals in the figure are observed for $n=1$, 3, and 5 reflecting the fourfold rotational symmetry of the orbits. Misalignments of only 2° are sufficient to destroy this symmetry and produce additional CPR at the even harmonics of the fundamental. Taking the resonance condition as being satisfied at maximum transmission, the effective mass ratio is calculated from Eq. (2.15) as $m^*/m_0 = 1.35$, very close to that observed in Fig. 2 at k_2.

Shown in Fig. 6 are data from a thicker sample,

1.70×10^{-2} cm ,

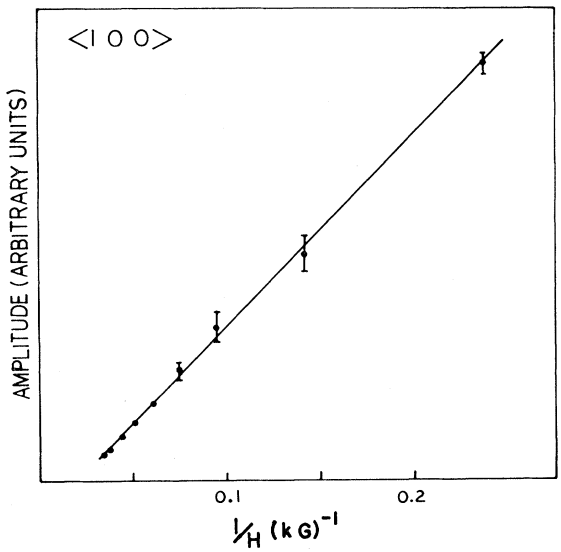

FIG. 4. Amplitude of the GKO signal in Fig. 3 as a function of $1/H$.

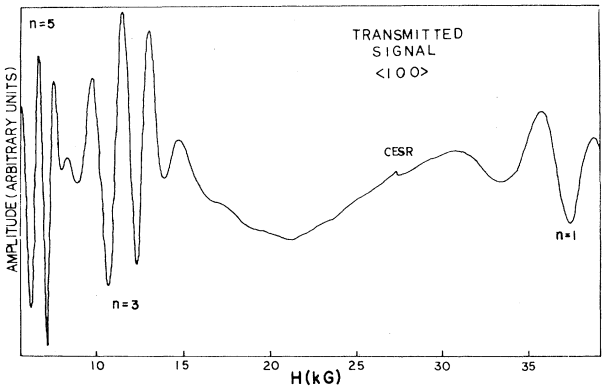

FIG. 5. Transmitted signal for a ⟨100⟩ sample of thickness 0.0038 cm and resistivity ratio 1000.

with a resistance ratio of 4200. This resistance ratio is sufficiently high that even the belly electrons can traverse the sample without scattering. Both the CTE and the EHT variety of oscillation are clearly seen superimposed on each other in the figure. It should be noted that the CPR signals do not have line shapes symmetric about their centers as predicted by Eq. (4.3), but rather fall to zero considerably more rapidly on the high-field side than on the low-field side of each peak. This may be due to the rather large fraction of Fermi-surface area having a mass of $m^* \approx 1.35 m_0$ [Fig. 2(a)], and the necessity of doing a more careful integration over k_H in obtaining that equation. In fact, such an attempt by PBS to do a more detailed integration does indeed produce signals having a more extensive low-field tail (see Fig. 14 in Ref. 4). Another interesting feature in the data not easily explained by the model is the fact that in general the amplitude of the harmonics of CPR is larger than that of the fundamental resonance itself. A possible explanation is that in the vicinity of the fundamental CPR, the effective electrons within the anomalous skin depth are resonant themselves and are able to more efficiently screen out the rf driving fields from the sample.

The data reported so far are generally in good agreement with earlier experimental results. Table I gives a numerical comparison of our results with the predictions of the model and the data of PBS and Perrin *et al.*

B. ⟨110⟩ orientation

In this geometry the ⟨110⟩ crystal axis is normal to the sample plane and the electron orbits have two-fold rotational symmetry.

1. Theoretical predictions

Figure 7 shows a plot for this new orientation of the same orbital parameters m^*, $\bar{v}_H$, $(\partial A/\partial k_H)_E$, and T_1 as a function of $k_H/k_{\rm FE}$. In this case, electrons on equatorial and polar orbits pass over the necks and only those which lie in the range

$$0.2 \lesssim k_H/k_{\rm FE} \lesssim 0.8$$

avoid them. As can be seen from the figure, m^*, $\bar{v}_H$, and $(\partial A/\partial k_H)_E$ do not vary all that much over this range of k_H, and as a consequence different types of GKO signals may be hard to separate and distinguish from each other. In particular, varying the sample thickness is not likely to be as useful as it was for ⟨100⟩ specimens.

The topological effectiveness does not have any sharp peaks as previously. However, the dashed straight-line approximation is of the type we considered earlier in Fig. 1(b), and from which we ex-

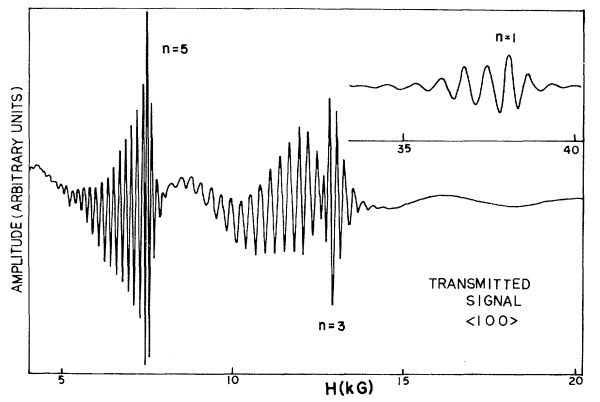

FIG. 6. Transmitted signal for a ⟨100⟩ sample of thickness 0.0170 cm and resistivity ratio 4200.

TABLE I. Numerical data for ⟨100⟩ orientation.

Type of signal	Model	$\frac{1}{n}\left[\frac{\partial A}{\partial k_H}\right]_E$ (Å^{-1}) This work	PBS[a]	Perrin *et al.*[b]
CTE, $n=1$	8.60	8.76±0.10[c]	8.60	
EHT, $n=1$	2.20	2.08±0.06[d]	2.10	2.3
EHT, $n=3$	0.73	0.77±0.04[d]		0.76
EHT, $n=5$	0.44	0.47±0.03[d]		
m^*/m_0 (CPR)	1.37	1.35±0.01[e]	1.34±0.01	

[a]Reference 4.
[b]Reference 3.
[c]One sample.
[d]Average of four samples.
[e]Average of seven samples.

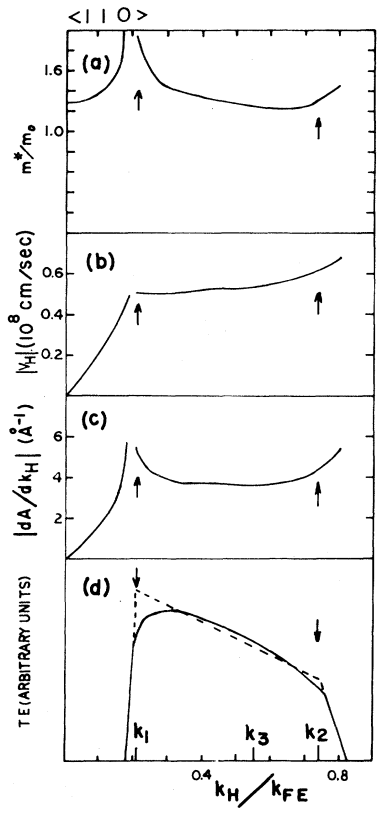

FIG. 7. Fermi-surface parameters for the ⟨110⟩ orientation of copper. Arrows at k_1 and k_2 indicate orbits leading to CTE oscillations.

pect [Eq. (2.14)] a superposition of two oscillatory GKO's of the CTE type—one due to the electron orbit at $k_1=0.21k_{FE}$ and the other due to the orbit at $k_2=0.74k_{FE}$ (see figure). From the figure we find that

$$(\partial A/\partial k_H)_E=5.0\ \text{Å}^{-1}$$

at k_1 and 4.4 Å^{-1} at k_2. Thus the periods of the two oscillations should differ by about 12%, with that coming from the orbit at k_1 being the lower-frequency oscillation [Eq. (2.17b)]. As $m^*(k_H)$ is changing reasonably fast with k_H at both k_1 and k_2, CPR is not predicted for either of these GKO's. Since $\bar{v}_H$ is reasonably constant at k_1, we can repeat our arguments used for the ⟨100⟩ direction and predict that the amplitude of the lower-frequency CTE oscillation will vary approximately as $1/H$ [see Eq. (4.2)]. Because neither the effective mass nor $\bar{v}_H$ is constant at k_2, no simple approximation for the line shape can be made in this case.

A shallow minimum in $(\partial A/\partial k_H)_E$ appears at $k_3=0.55k_{FE}$. Although the effective mass is not constant here, it is changing slowly with k_H, and consequently one would expect an EHT-type oscillation due to an electron orbit in this vicinity and perhaps also a weak and broad CPR. The value of $(\partial A/\partial k_H)_E$ at k_3 is 3.7 Å^{-1}. If we approximate m^* and $\bar{v}_H$ as being constant at k_3, then an equation similar to Eq. (4.3) describes the line shape predicted for the CPR. Twofold rotational symmetry of the orbits again leads to values of $n=1, 3, 5, 7, \ldots$ in that equation.

2. *Experimental observations*

Figure 8 displays the transmitted signal at higher magnetic fields (25—45 kG) in a sample

$$2.10\times10^{-2}\ \text{cm}$$

in thickness and having a resistance ratio of 2500. Figure 9 is a continuation of the data from the same sample at lower fields (8—25 kG). This particular thickness is the largest we have studied for this orientation. As indicated by the dashed lines, the data in Fig. 8 consists of two types of signals—an oscillation of decreasing amplitude but constant period extending the full range of the field sweep, superimposed on which is a resonance-type signal which reaches maximum amplitude near 35 kG. The period of the oscillations within the resonance signal is about 15% less than that of the other signal. From these two periods we calculate $(\partial A/\partial k_H)_E=3.64$ Å^{-1} and 4.26 Å^{-1}.

In Fig. 9 the 4.26 Å^{-1} oscillation is still seen on the high-field side of the trace. However, for fields less than 20 kG, another oscillation of still larger period appears, from which $(\partial A/\partial k_H)_E$ is calculated to be 4.94 Å^{-1}. This last signal, whose amplitude increases with lower fields, is complicated by the appearance of an additional "fine structure" which becomes quite strong below 12 kG.

These three main oscillations can be identified as

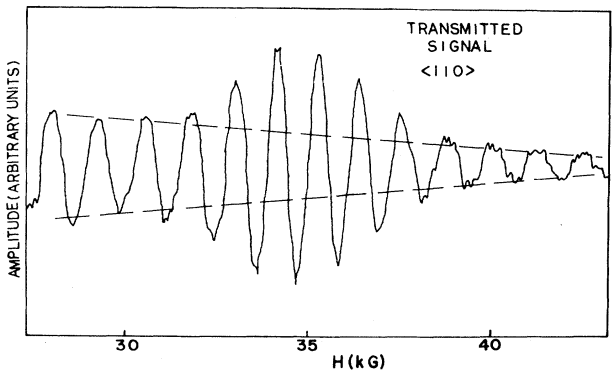

FIG. 8. Transmitted signal at higher magnetic fields for a ⟨110⟩ sample of thickness 0.0210 cm and resistivity ratio 2500.

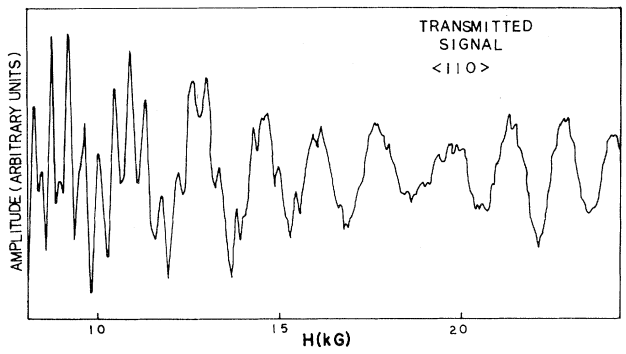

FIG. 9. Transmitted signal at lower magnetic fields for the sample of Fig. 8.

the GKO signals expected from electron orbits at k_1, k_2, and k_3 in Fig. 7. The lowest-field signal is the CTE variety of oscillation due to the orbit at k_1. As predicted, its amplitude falls off approximately as $1/H$ due to the constant value of $\bar{v}_H$ at k_1. This explains its dominance at low field. The other CTE oscillation arising from electrons at k_2 is that which extends over the full 20-kG field sweep of Fig. 8. The resonant peak near 35 kG is identified as the fundamental ($n=-1$) CPR of the EHT signal originating from electrons at k_3. The center of this peak gives an effective mass of $m^*=1.23m_0$, very close to the predicted value of $1.22m_0$ [Fig. 7(a)]. The spacing of the oscillations within this peak is also in close agreement to that predicted by the model. The fine-structure oscillations below 12 kG appear to be the $n=3$ and $n=5$ harmonics of the CPR, but they are not easily identified in some samples because of the complicated interference of signals taking place in this region.

The location in the magnetic field of the oscillations due to the orbit at k_2 can be explained by the PBS model. According to Eq. (2.14) the amplitude of this CTE signal is proportional to $(q'L)^{-1}$ evaluated at k_2. For the fundamental oscillation ($n=-1$) we have

$$\frac{dq}{dk_H}=\frac{\omega}{\bar{v}_H}\left[\frac{\omega_c}{\omega}\left[\frac{1}{m^*}\frac{dm^*}{dk_H}+\frac{1}{\bar{v}_H}\frac{d\bar{v}_H}{dk_H}\right]-\frac{(1+i/\omega\tau)}{\bar{v}_H}\frac{d\bar{v}_H}{dk_H}\right]. \tag{4.4}$$

This gives a maximum amplitude when

$$\frac{\omega_c}{\omega}=\frac{(1/\bar{v}_H)(d\bar{v}_H/dk_H)}{(1/m^*)(dm^*/dk_H)+(1/\bar{v}_H)(d\bar{v}_H/dk_H)}. \tag{4.5}$$

From the computer plots of Fig. 7 we find that

$$\frac{1}{m^*}\frac{dm^*}{dk_H}\approx\frac{1}{\bar{v}_H}\frac{d\bar{v}_H}{dk_H}. \tag{4.6}$$

Putting this result into Eq. (4.5) we see that this CTE signal will be largest when $\omega_c/\omega\approx\frac{1}{2}$, thus explaining its strongest appearance at fields higher than that of the other CTE oscillation but less than that of the CPR of the EHT signal.

As one goes to thinner samples, these three main oscillations can still be seen for a while, although the lowest-field signal becomes obscured by very strong fine structure. In the thinnest sample (2×10^{-3} cm) only the fundamental CPR near 35 kG can be identified. Table II summarizes the data for this particular geometry.

C. ⟨111⟩ orientation

In this geometry the ⟨111⟩ crystal axis is normal to the sample plane and the electron orbits have threefold rotational symmetry.

1. Theoretical predictions

Figure 10 shows the same orbital parameters as given previously for the other crystallographic orientations. For this situation, electrons whose orbits lie in the range

$$0.2\lesssim k_H/k_{\mathrm{FE}}\lesssim0.55$$

encounter three necks with each orbit around the Fermi surface. The topological effectiveness increases gradually as one progresses from polar orbits towards the equator, but shows a sharp cutoff as the necks are approached. This is again similar to the situation considered in Fig. 1(a). The maximum in the topological effectiveness just prior to the cut-

TABLE II. Numerical data for ⟨110⟩ orientation.

Type of signal	Model	$\frac{1}{n}\left[\frac{\partial A}{\partial k_H}\right]_E$ (Å^{-1}) This work	Perrin *et al.*[a]
CTE at k_1, $n=1$	5.00	5.00±0.10[b]	
CTE at k_2, $n=1$	4.40	4.26±0.08[b]	
EHT, $n=1$	3.70	3.64±0.06[d]	3.70
EHT, $n=3$	1.23	1.43±0.02[c]	
EHT, $n=5$	0.74	0.80±0.01[c]	0.735
m^*/m_0 (CPR)	1.22	1.23±0.01[b]	

[a]Reference 3.
[b]Average of four samples.
[c]Average of three samples.
[d]Average of two samples.

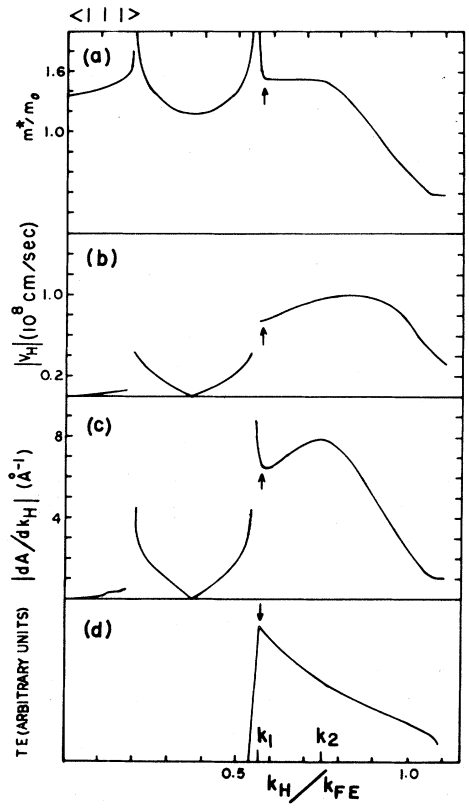

FIG. 10. Fermi-surface parameters for the ⟨111⟩ orientation of copper. Arrows at k_1 indicate an orbit leading to a CTE oscillation.

off occurs at $k_1=0.57\ k_{FE}$ and the corresponding value of $(\partial A/\partial k_H)_E$ is 6.3 Å^{-1}. From the figure we also see a minimum in the quantity $(\partial A/\partial k_H)_E$ very close to this same region. Consequently, at k_1 two mechanisms are operating (CTE and EHT), which should produce an exceptionally strong GKO. The effective mass at k_1 is such that its slope (dm^*/dk_H) is changing very rapidly with k_H, which can lead to a shift in field at which the maximum signal occurs. Because our equation for the CTE variety of GKO [Eq. (2.13)] breaks down when

$$d/dk_H(\partial A/\partial k_H)_E \rightarrow 0\ ,$$

we recover Eq. (2.11) for EHT oscillations as the appropriate one to describe this situation. The amplitude of the signal is thus proportional to $(q''L)^{-1/2}$. Making use of the fact that at k_1

$$\frac{dm^*}{dk_H}\approx\frac{d\bar{v}_H}{dk_H}\approx 0\ , \tag{4.7}$$

we obtain

$$q''=\frac{-1}{\bar{v}_H^2}\left|\frac{d^2\bar{v}_H}{dk_H^2}\right| \times\left[\omega+\frac{i}{\tau}+n\omega_c\left[1+\frac{\frac{1}{m^*}\left|\frac{d^2m^*}{dk_H^2}\right|}{\frac{1}{\bar{v}_H}\left|\frac{d^2\bar{v}_H}{dk_H^2}\right|}\right]\right]\ . \tag{4.8}$$

This gives rise to a resonance behavior in the amplitude, but one which occurs at lower magnetic fields than that given by the usual condition in Eq. (2.15). Such shifts should not be important for the ⟨100⟩ and ⟨110⟩ orientations where dm^*/dk_H is changing very slowly at the dominant orbits.

Another EHT-type signal can appear in the vicinity of $k_2=0.74k_{FE}$ where

$$(\partial A/\partial k_H)_E=7.9\ \text{Å}^{-1}\ .$$

However, since m^* is not constant here and the topological effectiveness is smaller, we expect a considerably weaker oscillation from this orbit. From the threefold rotational symmetry of the orbits, Eq. (2.5) predicts harmonics of the various GKO signals given by $n=1,2,4,5,7,\ldots$.

According to the low-frequency measurements of Perrin *et al.*,[3] two other EHT signals can also be obtained from the belly-orbit region. However, in this vicinity $\bar{v}_H$ and $(\partial A/\partial k_H)_E$ are small and m^* is not constant. Thus we would only expect these oscillations to show up as a weak "fine structure" in the thinnest samples.

2. *Experimental observations*

In Fig. 11 transmission data is shown for a thick sample (3.70×10^{-2} cm) having a resistance ratio of 6500. Very strong oscillations are observed for magnetic fields larger than 36 kG. The constant spacing between the peaks gives

$$(\partial A/\partial k_H)_E=6.3\ \text{Å}^{-1}\ ,$$

making this signal obviously the one predicted from electron orbits near k_1 in Fig. 10. It should be noted that these oscillations have a maximum value around 38 kG and not the 44 kG that one might predict from the effective mass ratio of 1.55 in this vicinity of k_H. This is in agreement with Eq. (4.8) which predicts the signal maximum to be displaced to lower fields because of the rapid change of dm^*/dk_H at k_1. The second maximum at 47 kG, which disappears in thinner samples, does not correspond to $m^*=1.55m_0$ and may represent a beating taking place between two or more of the predicted GKO signals. It is of interest to note that this sig-

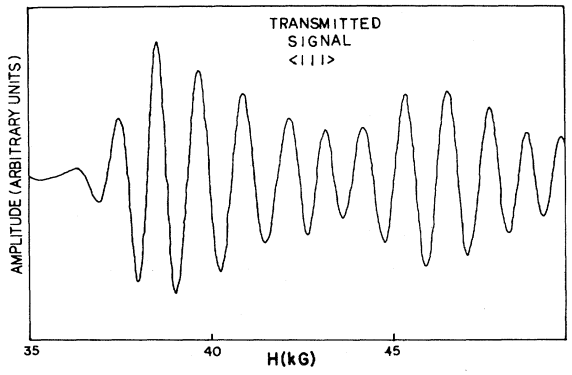

FIG. 11. Transmitted signal at higher magnetic fields for a ⟨111⟩ sample of thickness 0.0370 cm and resistivity ratio 6500.

nal which has an extended tail on the high-field side, results from a *minimum* in $(\partial A/\partial k_H)_E$, while the CPR signals in the ⟨100⟩ orientation, which have extended tails on the low-field side of the peak, result from a *maximum* in $(\partial A/\partial k_H)_E$.

Figure 12 displays the transmission signal at lower fields (10—25 kG) for the same sample as above. These signals are considerably weaker, and the gain has been increased by a factor of 50 over that used in Fig. 11. The low-field transmission is quite complicated and is a combination of several oscillations. From the calculated values of $(\partial A/\partial k_H)_E$ some of these oscillations are higher harmonics due to the orbit at k_2 in Fig. 10. The fundamental oscillation due to this orbit is not seen, but may be obscured by the very strong oscillations from the k_1 orbit seen in Fig. 11. A number of thinner samples have also been checked for this orientation. All of them show very strong oscillations at high field due to the k_1 orbit. The low-field transmission becomes much stronger in the thinner samples, but too complicated for analysis. In no

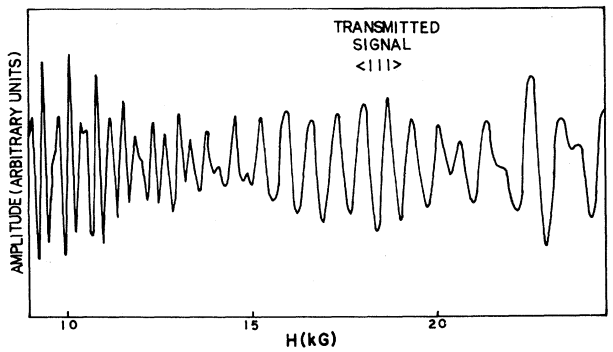

FIG. 12. Transmitted signal at lower magnetic fields for the sample of Fig. 11. The vertical gain has been increased by a factor of 50 over that used in Fig. 11.

TABLE III. Numerical data for ⟨111⟩ orientation.

Type of signal	Model	$\frac{1}{n}\left[\frac{\partial A}{\partial k_H}\right]_E$ (Å^{-1}) This work	Perrin *et al.*[a]
CTE, $n=1$	6.30	6.28±0.07[b]	
CTE, $n=4$	1.58	1.52±0.04[c]	
EHT, $n=1$	7.90		7.6
EHT, $n=2$	3.95	4.03±0.04[d]	
EHT, $n=4$	1.98		1.8

[a]Reference 3.
[b]Average of five samples.
[c]Average of four samples.
[d]Average of three samples.

case are we able to unambiguously identify any of the EHT oscillations due to orbits near the equator. A summary of the calculated parameters is given in Table III.

D. Polarization

As explained in Sec. III, the polarization (linear or circular) of the transmission signal can be determined by observing the behavior of the signal as the phase of the microwave reference is varied [Eqs. (3.2) and (3.3)]. For high magnetic fields this polarization is circular for all three crystal orientations. The polarization at low fields is very difficult to determine because of the complicated nature of the signals (superposition of several varieties), and has only been determined for the ⟨100⟩ orientation in thick samples, for which everything but the fundamental CTE signal can be eliminated. Figure 13 shows data extending to zero field for such a sample. For this sample the CTE oscillation, as described previously, extends down to about 5 kG. These oscillations display the property of circular polarization in that they shift linearly in field with rotation of the phase of the microwave reference. Below 5 kG, however, the signal changes character and displays the property of a linearly polarized signal—namely, the oscillations stay fixed in field and their amplitude varies with rotation of the reference phase.

V. CONCLUSION

GKO signals have been studied at microwave frequencies in single-crystal plates of copper oriented along the ⟨100⟩, ⟨110⟩, and ⟨111⟩ crystal axes. As we have seen, the theoretical model originally proposed by Phillips, Baraff, and Schmidt to explain such data for a ⟨100⟩ orientation is also very useful in interpreting experimental data taken for the other two orientations. The model allows one to identify those orbits on the Fermi surface that contribute to

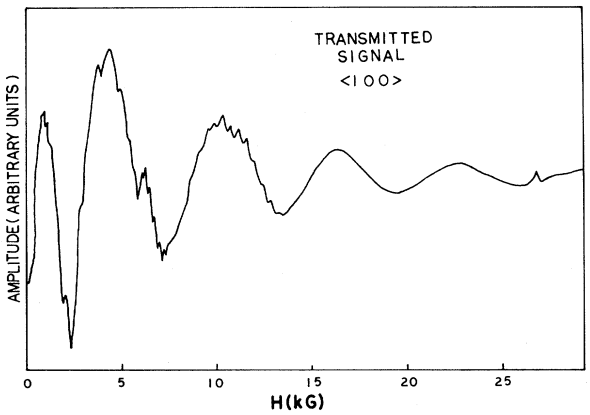

FIG. 13. Transmitted signal for a ⟨100⟩ sample of thickness 0.0095 cm and resistivity ratio 1200.

the observed signals and to predict, at least qualitatively, the signal amplitude as a function of magnetic field. In copper we find two classes of signals: (a) those arising from a sharp cutoff of the topological effectiveness, and (b) those due to an extremal helical trajectory. Harmonics of the fundamental oscillations are explained in terms of noncircular orbits having various degrees of rotational symmetry. The model accounts for cyclotron phase resonance in terms of certain regions of the Fermi surface where the effective mass is reasonably constant. One feature which the model cannot explain is the production of circularly polarized signals at higher magnetic fields while the driving fields themselves are linearly polarized.

ACKNOWLEDGMENTS

This research project was supported in part by National Science Foundation Grant No. DMR-7913786. We are happy to thank S. Schultz for providing high-purity copper single crystals and G. A. Baraff for the use of certain computer programs and theoretical discussions. We would also like to acknowledge the technical assistance of M. R. Pattison on the microwave spectrometer, and helpful information on the Fermi surface of copper from J. D. Gavenda.

*Present address: Department of Physics, National Central University, Chung-li, Taiwan 320, Republic of China.

[1]G. L. Dunifer, T. M. Hsu, and M. R. Pattison (unpublished).

[2]V. F. Gantmakher and E. A. Kaner, Zh. Eksp. Teor. Fiz. 48, 1572 (1965) [Sov. Phys.—JETP 21, 1053 (1965)].

[3]B. Perrin, G. Weisbuch, and A. Libchaber, Phys. Rev. B 1, 1501 (1970).

[4]T. G. Phillips, G. A. Baraff, and P. H. Schmidt, Phys. Rev. B 5, 1283 (1972).

[5]D. Pinkel, G. L. Dunifer, and S. Schultz, Phys. Rev. B 18, 6658 (1978).

[6]J. D. Gavenda and C. M. Casteel, Phys. Rev. B 19, 4331 (1979).

[7]T. G. Phillips, G. A. Baraff, and G. L. Dunifer, Phys. Rev. Lett. 30, 274 (1973).

[8]C. C. Grimes and A. F. Kip, Phys. Rev. 132, 1991 (1962).

[9]M. Elliott and W. R. Datars, J. Phys. F 12, 465 (1982).

[10]W. R. Datars, private communication.

[11]J. J. Gniewek and A. F. Clark, J. Appl. Phys. 36, 3358 (1965).

[12]G. L. Dunifer and M. R. Pattison, Phys. Rev. B 14, 945 (1976).

[13]G. L. Dunifer, M. R. Pattison, and T. M. Hsu, Phys. Rev. B 15, 315 (1977).

[14]D. A. H. Mace, J. R. Sambles, and G. L. Dunifer (unpublished).

[15]M. R. Halse, Philos. Trans. R. Soc. London A265, 507 (1969).